Droplet behavior of non-equilibrium condensation in the supersonic separator

Wang, Chao; Wang, Xiaotong; Ding, Hongbing; Cao, Peijuan; Wen, Chuang

Published in:
Proceedings of the 2018 IEEE International Instrumentation and Measurement Technology Conference (I2MTC)

Link to article, DOI:
10.1109/I2MTC.2018.8409609

Publication date:
2018

Document Version
Peer reviewed version

Droplet Behavior of Non-equilibrium Condensation in the Supersonic Separator

Chao Wang, Xiaotong Wang, Hongbing Ding*, Peijuan Cao
Tianjin Key Laboratory of Process Measurement and Control, School of Electrical and Information Engineering Tianjin University, Tianjin 300072, China
Corresponding author e-mail: hbding@tju.edu.cn

Chuang Wen
Department of Mechanical Engineering, Technical University of Denmark, Nils Koppels Allé, 2800 Kgs. Lyngby, Denmark
e-mail: cwen@mek.dtu.dk

***Abstract*—Supersonic swirling separation plays an important role in the separation of the water vapor and heavy hydrocarbons in natural gas processing. A viscous flow solver with slip model was developed to predict the non-equilibrium condensation phenomenon in supersonic separator. Several sets of experiments were conducted to validate the accuracy of numerical models. The detailed introduction of the experimental device was discussed. Then, to investigate the behavior of gas-droplet two-phase flow with strong swirls, the tangential velocity and centrifugal acceleration were simulated. Moreover, the distributions of droplet number density and bulk density of dispersed droplet phase in the supersonic separator were discussed in detail.**

Keywords—natural gas processing; supersonic separator; non-equilibrium condensation; slip model

I. INTRODUCTION

The separation of the water vapor and heavy hydrocarbons is an essential procedure in natural gas processing. As an emerging gas separation technology, the supersonic swirling separation has been more widely adopted in recent years. The supersonic separator is mainly comprised of 4 parts, namely, the Laval nozzle, the vortex generator, the liquid exit and the diffuser [1]. Compared to the conventional gas separation technologies, the key advantage of this unique technique consists in its simple and compact tubular structure without any moving parts [2]. Therefore, the supersonic swirling separation conforms to the development requirements of gas processing including safety, high efficiency, environmental protection and economical operation [3].

The research of supersonic swirling separation has received increasing attention in recent years. The first generation of supersonic separator, Twister Mark I, was designed by Twister B.V. in 2000 [4]. The structures of circular nozzle and pre-type vortex generator were adopted in Twister Mark I. To improve efficiency in the term of liquid recovery, the design of the nozzle was optimized into the annular nozzle with inner body by Prast [5]. With in-depth research, to reduce the pressure loss and energy loss across the device, Schinkelshoek [6] redesigned the vortex generator and moved it to subsonic region.

Along with the rapid development of CFD technology, numerical simulation has been broadly used in the research of supersonic swirling separation [7]. Through numerical method, Wen discussed the effect of structure of vortex generator [8], the shape of diffuser [9] and the length of cyclonic separation section [10] on the collection efficiency in a supersonic separator. Based on the heterogeneous nucleation, Ma [11] proposed a droplet enlargement method of supersonic swirling separation. Moreover, Karimi [12], Jiang [13], Shahsavand [14] and Alfyorov [15] did plenty of researches in the physical designs and sensitivity to flow conditions through analytical, numerical, and experimental methods.

This work is supported by National Natural Science Foundation of China under Grant 61627803, 51506148 and 61673291, Natural Science Foundation of Tianjin under Grant 16JCQNJC03700 and 15JCYBJC19200.

II. SUPERSONIC SEPARATOR

According to the previous researches, there are mainly two structures of supersonic separator, namely Twister Mark I and Twister Mark II [11]. As shown in Fig.1 (a), the hollow tube structure is adopted in Twister Mark I and the vortex generator is designed as a delta wing. The device of Twister Mark II, plotted in Fig.1 (b), is consisted of the annular nozzle with inner body and the vortex generator made up of a set of helical blades.

The efficiency in the term of liquid recovery is the key characteristic in the research of supersonic separators. However, for different structures of supersonic separator, the research directions are slightly distinct [8].

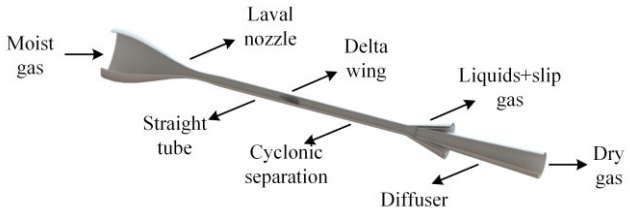

(a) Twister Mark I

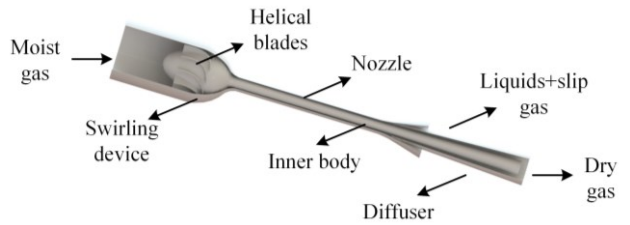

(b) Twister Mark II
Fig.1 Structures of supersonic separators

For Twister Mark I, the shape and location of the delta wing are the key characteristics [10]. Thus the tangential velocity downstream the delta wing and the length of the cyclonic separation section are the valuable research issues [16]. In addition, the vortex generator is located at the supersonic region of the gas flow, and therefore the pressure loss and energy loss are taken into account in the related studies.

For Twister Mark II, the helical blades and the inner body are the critical designs. The effect of blade numbers and blade

angles on gas swirling characteristics is the concerned topic [8]. Due to the existence of the inner body, the non-equilibrium condensation phenomenon is complicated and still not fully understood as a result of the complex phase change process. The non-equilibrium condensation of moist air is widely used as a means of studying the non-equilibrium condensation phenomenon in the supersonic separator [11],[17]. In this paper, the non-equilibrium condensation of moist air in the Twister Mark II supersonic separator is numerically analyzed using a viscous flow solver with slip model. The droplet behavior of non-equilibrium condensation is discussed in detail.

III. Physical Model

A. Mathematical Model

The mass and momentum conservation equations for the continuous phase are calculated by

$$\frac{\partial(\rho_g(1-\alpha))}{\partial t}+\frac{\partial}{\partial x_j}\left(\rho_g(1-\alpha)u_{gj}\right)=-\Gamma_1-\Gamma_2 \tag{1}$$

$$\frac{\partial}{\partial t}\left(\rho_g(1-\alpha)u_{gi}\right)+\frac{\partial}{\partial x_j}\left(\rho_g(1-\alpha)u_{gj}u_{gi}+(1-\alpha)p_g\delta_{ij}\right)=-\Gamma_2 u_{\mathrm{int}\,j}-F_{Dj}-p_{\mathrm{int}}\frac{\partial\alpha}{\partial x_j} \tag{2}$$

where, ρ, u, p, x, α and δ_{ij} are density, velocity, pressure, Curvilinear coordinate, dispersed phase volume fraction and Kronecker delta function, respectively. The subscripts 'i' and 'j' are the tensor notations. The subscripts 'g', 'm' and 'int' refer to continuous phase, mixture component and interphase component, respectively. $u_{\mathrm{int}j}$ and F_{Dj} describe the interphase velocity component and the resisting force per mixture volume unit [18]

$$u_{\mathrm{int}\,j}=\frac{\rho_l u_{lj}\alpha+\rho_g u_{gj}(1-\alpha)}{\rho_m} \tag{3}$$

$$F_{Dj}=\frac{9\mu\alpha}{2r^2(1+2Kn(1.257+0.4e^{-1.1/2Kn}))}(u_{gj}-u_{lj}) \tag{4}$$

where, r, μ and Kn are droplet radius, viscosity and Knudsen number, respectively. The subscripts 'l' refers to the dispersed phase.

The energy conservation equation for the continuous phase is computed by

$$\frac{\partial}{\partial t}\left(\rho_g(1-\alpha)E_g\right)+\frac{\partial}{\partial x_j}\left(\rho_g(1-\alpha)u_{gj}H_g\right)=-\Gamma_2(H_{g\,\mathrm{int}}-L)-u_{\mathrm{int}\,j}F_{Dj}-p_{\mathrm{int}}u_{\mathrm{int}\,j}\frac{\partial\alpha}{\partial x_j} \tag{5}$$

where, E, h and H are energy, static enthalpy and total enthalpy, respectively.

The dispersed phase is the droplet totally formed by non-equilibrium condensation, which could be described by the following conservation equations

$$\frac{\partial(\rho_l\alpha)}{\partial t}+\frac{\partial}{\partial x_j}\left(\rho_l\alpha u_{lj}\right)=\Gamma_1+\Gamma_2 \tag{6}$$

$$\frac{\partial}{\partial t}\left(\rho_l\alpha u_{li}\right)+\frac{\partial}{\partial x_j}\left(\rho_l\alpha u_{lj}u_{li}+\alpha p_l\delta_{ij}\right)=\Gamma_2 u_{\mathrm{int}\,j}+F_{Dj}+p_{\mathrm{int}}\frac{\partial\alpha}{\partial x_j} \tag{7}$$

The source terms are computed by

$$\Gamma_1=\frac{4}{3}\pi\rho_l\rho_m r^{*3}J \tag{8}$$

$$\Gamma_2=4\pi\rho_l\rho_m nr^2\frac{dr}{dt} \tag{9}$$

where, J and r^* are nucleation rate and critical radius.

The turbulence of continuous phase is modeled by k-ε model, and the turbulent dispersion of droplets is not considered in the present slip model.

More details about the definitions of parameters and equations could be found in our previous works [19],[20].

B. Geometry and Mesh

In the present research, the major concern is the condensing process in the swirling flow and the distributions of condensing droplets in separation part. Thus, the liquid exit is not included in the present designed supersonic separator, as plotted in Fig.2. Furthermore, for the current structure, it is conducive to compare the characteristics of gas flow field in the separation part and in the diffuser.

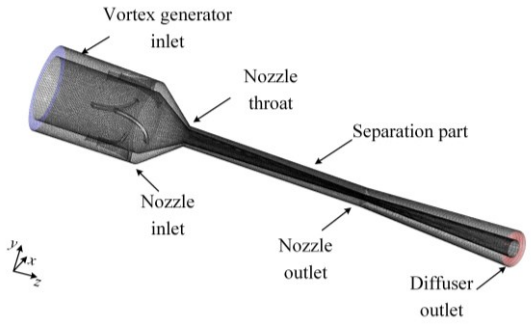

Fig.2 The geometry of designed supersonic separator

There are 6 helical blades in the vortex generator. The dimension parameters of designed supersonic separator are given in Table I. To illustrate the details of the inner body, only the meshes of face elements are shown in Fig.2. For the irregular structure of the helical blades, the unstructured tetrahedral meshes are adopted in the vortex generator. The structured hexahedral meshes are used in the other parts. To satisfy the grid independence, the numbers of unstructured and

structured meshes are 290473 and 491400, respectively.

TABLE I DIMENSION PARAMETERS OF DESIGNED SUPERSONIC SEPARATOR

Parameter	*Value(mm)*	*Value of z-axis coordinate*
Vortex generator inlet diameter (Inner body)	80 (60)	-100
Nozzle inlet diameter (Inner body)	80 (60)	0
Nozzle throat diameter (Inner body)	20 (14)	40
Nozzle outlet diameter (Inner body)	20 (6)	240
Diffuser outlet diameter (Inner body)	40 (20)	428
Nozzle converging length	40	-
Nozzle diverging length	200	-
Diffuser length	188	-

C. Numerical Scheme

The governing equations are solved by the finite volume method and fully implicit solver. The SIMPLE algorithm is adopted to deal with the pressure-velocity coupling [21]. The Reynolds Stress Model is used to model the swirling flow in the supersonic separator [22]. The turbulent dispersion of droplets is not considered in the present slip model. The transient scheme is second order upwind or Adams-Bashforth scheme [23]. All nonlinear equations are linearized and solved by Algebraic Multigrid method [24]. The convergence criterion is the residual mean squares (RMS) of the order of 10^{-5} or lower. For boundary conditions, the pressure inlet, pressure outlet and adiabatic and no slip wall are adopted.

IV. EXPERIMENTAL VALIDATION

The experimental validation contains two parts. The first experimental validation was conducted on the multi-parameter adjustable humidification device at *Tianjin Key Laboratory of Process Measurement and Control*. The second experimental validation was accomplished by the experimental data of *Wyslouzil*.

A. Experimental Device

The experimental device, as plotted in Fig.3, is designed to adjust the pressure, temperature and humidity of the inlet air. The discharged air volume of each air compressor is 3.3 Nm^3/min and the discharged pressure is 850 kPa.

To ensure the purity of the air, the purification device consists of the degreaser, the congealer, the refrigerated dryer and the ultra-filter. The set pressure value was adjusted by the motorized valve and maintained by the regulator tank and self-operated pressure regulating valves. The capacity of the buffer bank is 2 m^3. The accuracy of pressure probe is 0.2% at the range of 0 ~ 800 kPa.

The tubular heater operated by a SCR regulator could adjust the air temperature ONLINE. The heating power is 25 kW, and the maximum design loading pressure is 1.6 MPa. Two Pt100 temperature sensors are used for the measurement and control of heating temperature, one in tubular heater and the other at the exit of heater. The temperature measurement range and accuracy of the Pt100 temperature sensor are -200 ~ 500 ℃ and 0.15 ℃. The researches of accurate temperature measurement were reported in the I^2MTC 2012 conference paper [25].

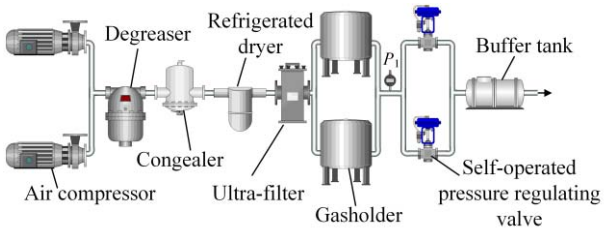

(a) Pure air generating device

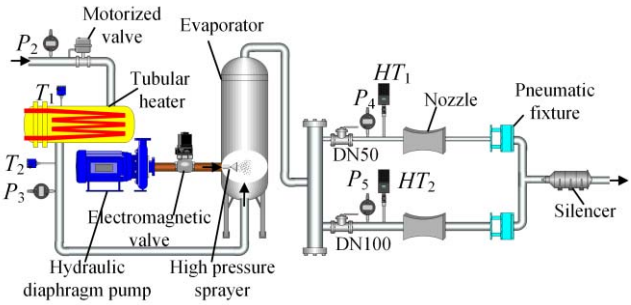

(b) Multi-parameter adjustable humidification device

Fig.3 Diagram of experimental device

The humidification device mainly consists of the hydraulic diaphragm pump, the high pressure sprayer, and the evaporator. The hydraulic diaphragm pump enhances the pressure of water. The high pressure water is forced out through the high pressure sprayer in small droplets with diameter of 1-15 μm. The range of the water volume flow-rate is from 0 to 17 L/h and the range of the water pressure is from 0 to 12.4 MPa. Through the heat absorption and evaporation process of the droplets, the humidity of air increases. The evaporation of droplets plays an extremely important role in the process of humidification. The evaporator is designed to ensure the uniformity and sufficiency of air. The droplets could be uniformly mixed with the air, and the humidifying effect is favorable. The quick response hygrometers of Vaisala HMP 110 (HT_1 and HT_2) are used to measure the humidity and temperature of the air in the gas pipeline. The temperature measuring range is from -40 ℃ to 80 ℃ with the accuracy of 0.2 ℃. The humidity measuring range, accuracy and response time are 0~100%RH, 1.5%RH and 10 s, respectively.

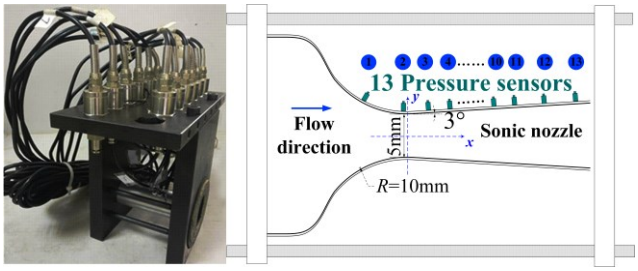

Fig.4 Pressure measuring device of sonic nozzle

The sonic nozzle and pressure measuring device are shown in Fig.4. The nozzle body is fixed with 13 pressure lead-in holes for the pressure measurement. 13 high-accuracy pressure probes were used to measure the time-averaged pressure distribution. The accuracy of pressure probe is 0.2% at the range of 0 ~ 800 kPa.

All the pressure probes are calibrated by the gas piston gauge device of National Primary Pressure Standard with the range of 0.005~10 MPa and expanded uncertainty of 0.0033% (k=2), to ensure the accuracy of the experimental pressure data.

B. *Validating by Experiments*

The three dimensional unstructured tetrahedral grids were adopted in the numerical simulations. To guarantee the grid independent solution, the grid size was performed as 106376. The inlet stagnation pressure p_0, temperature T_0 and relative humidity Φ_0 of the moist air are 300 kPa, 45 ℃ and 55 %RH. The comparison of numerical simulation and experiment for pressure distribution is plotted in Fig.5. The frozen flow refers to the gas flow without considering the condensation process. It is shown by calculation that the relative difference of pressure ratio between simulation and experiment is 4.61%. The pressure jump caused by latent heat released could be exactly predicted by the present numerical model [26].

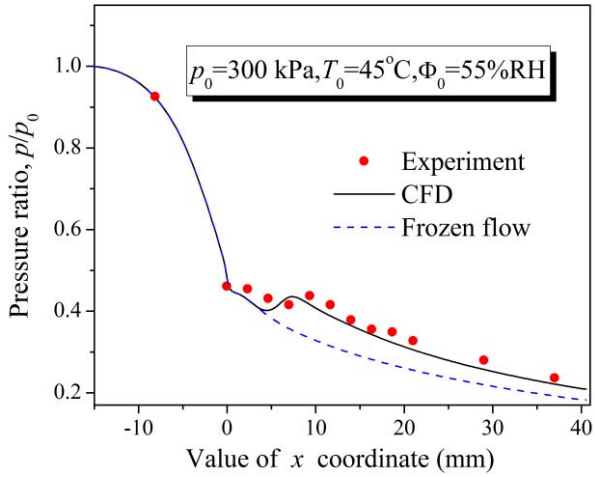

Fig.5 Comparison of simulation and experiment for pressure distribution

C. *Validating by Experiments of Wyslouzil*

The experimental validation was also accomplished by the experimental data of *Wyslouzil* [26]. The experimental device of *Wyslouzil* is plotted in Fig.6.

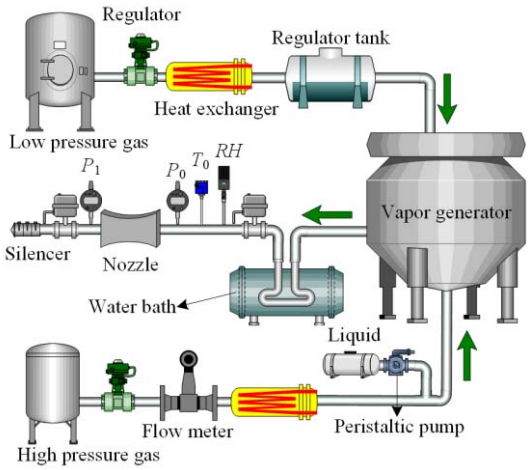

Fig.6 The experimental device of *Wyslouzil*

The carrier gas generation consists of two parts, namely the high pressure condensate-rich gas and low pressure dry gas. The temperature of the combined flow is adjusted by the water bath. The nozzle configuration is shown in Fig.7. A grid size of 19482 was performed to guarantee the grid independent solution.

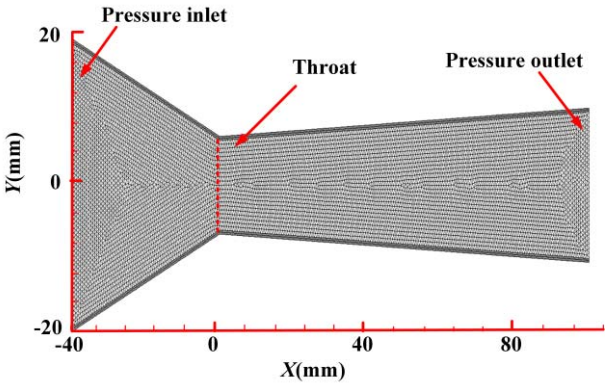

Fig.7 The configuration and mesh of the *Wyslouzil*'s nozzle

In the experiments of *Wyslouzil*, the stagnation pressure and stagnation temperature were invariant. Fig.8 shows the comparison between the numerical simulations and the experiments of *Wyslouzil* at different initial water partial pressures. The relative differences of p/p_0 between simulations and experiments are 1.93%, 2.86% and 2.91%, respectively. The results above indicated that the numerical model presented in the work can precisely predict the non-equilibrium condensation phenomenon of moist air.

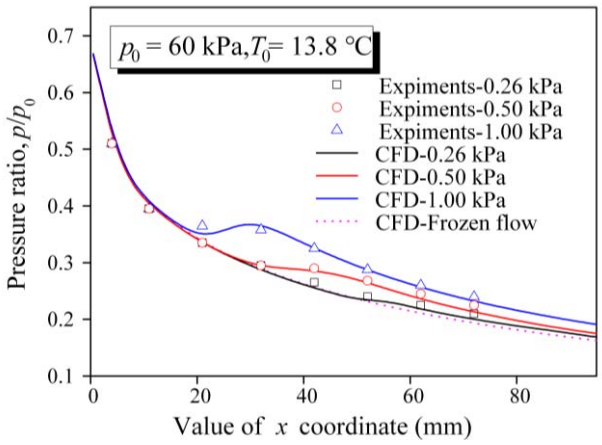

Fig.8 Comparison of numerical simulations and experiments of *Wyslouzil*

V. Results and Discussions

For non-equilibrium condensation in the supersonic separator, the numerical calculation is conducted at temperature of 13.8 ℃, inlet total pressure of 200 kPa, inlet water partial pressure of 1.50 kPa and outlet total pressure of 100 kPa.

The swirling motion is generated in the vortex generator. The tangential velocity of gas flow arises in the vortex generator and accelerates when the gas flow passes through the nozzle throat. On account of the tangential velocity, the strong

swirls are present in the gas flow field, as plotted in Fig.9. The maximum value of tangential velocity in the separation part is 65.4 m/s.

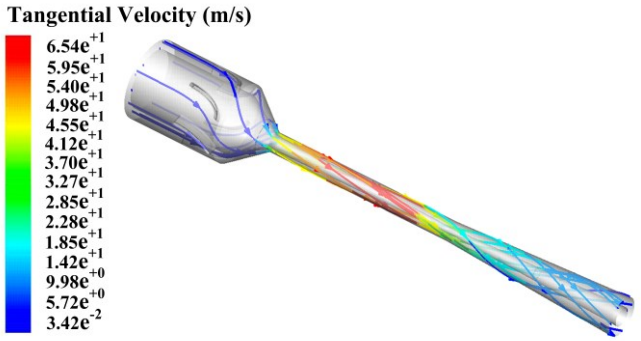

Fig.9 The gas flow field in the supersonic separator

The centrifugal acceleration of cross section at x = 0 is shown in Fig.10. In the separation part, the value of centrifugal acceleration is in the order of 10^5. It indicated that the sustained centrifugation exists in the separation part. For the gas-droplet two-phase flow, the strong sustained centrifugation will lead to the liquid droplets separation process.

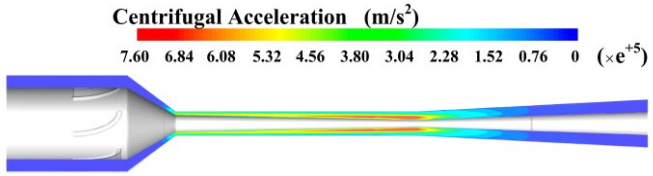

Fig.10 The centrifugal acceleration of cross section at x = 0

The gas flow travels through the supersonic separator with the process of temperature reduction. The nucleation process occurs in the downstream position of nozzle throat. As shown in Fig.11, the homogeneous nucleation ratio increases from 0 to $1.33 \cdot 10^{20}$ $m^{-3}s^{-1}$ and shows a rapid variation both in space and in time. With the influence of centrifugal effect, the liquid droplets formed by non-equilibrium condensation are separated from gas flow in the separation part.

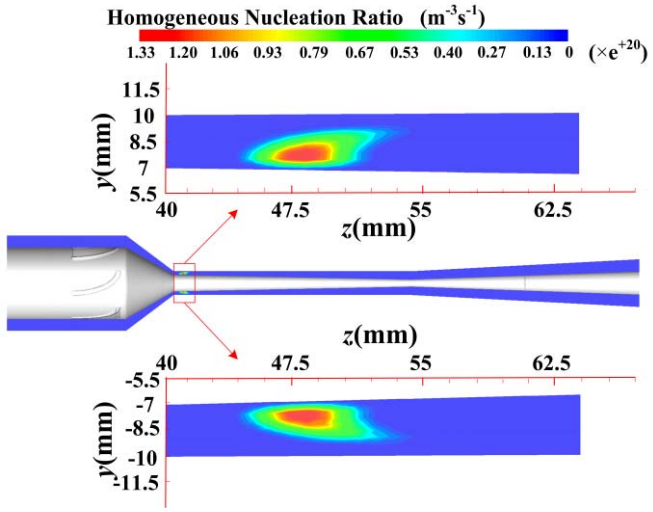

Fig.11 The homogeneous nucleation ratio of cross section at x = 0

The droplet behavior near the outlet of separation part at z = 220 is plotted in Fig.12. Due to the axisymmetric characteristics of the flow field, the distributions of droplet number density and bulk density of dispersed droplet phase are described in the direction of x = 0. The bulk density of dispersed droplet phase $\overline{\rho_l}$ is defined as:

$$\overline{\rho_l} = \rho_l \times \alpha \tag{10}$$

where, ρ_l is the density of droplet and α is the dispersed droplet phase volume fraction.

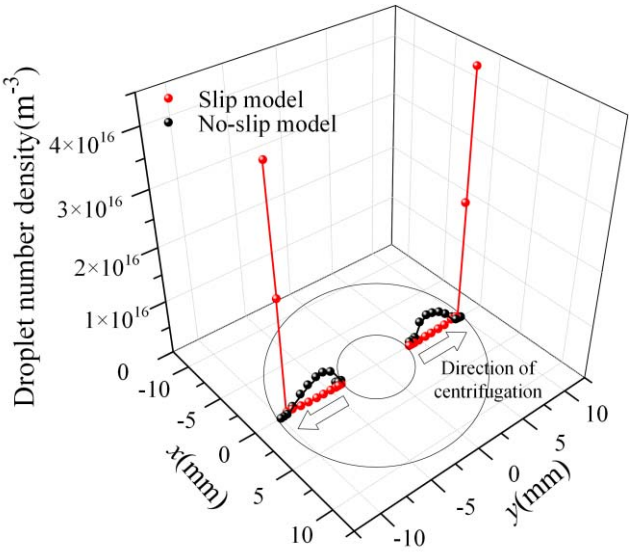

(a) Distributions of droplet number density

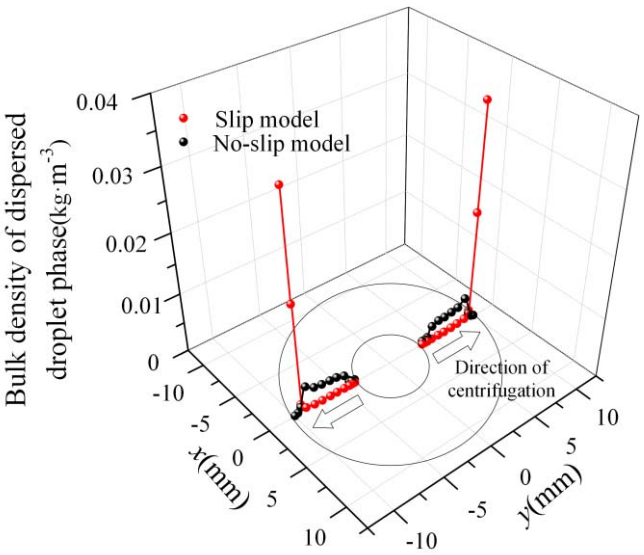

(b) Distributions of bulk density of dispersed droplet phase

Fig.12 Droplet behavior in the separation part

For the present slip model, the strong sustained centrifugation leads to the significant difference between the droplet behavior near the outside wall and that near the inside wall. The maximums of droplet number density and bulk

density of dispersed droplet phase near the outside wall are 4.47×10^{16} m^{-3} and 0.035 $kg\cdot m^{-3}$, while the minimums near the inside wall are 9.3×10^{8} m^{-3} and 6.26×10^{-9} $kg\cdot m^{-3}$, respectively. The no-slip model predicts the separation process without considering the interphase velocity component and resisting force [18] and it could not exactly describe the droplet behavior of non-equilibrium condensation in the supersonic separator as shown in Fig.12.

Through the comparison of two models, it indicated that the present slip model could predict the characteristic of separation of the gas-droplet two-phase flow in the supersonic separator.

VI. Conclution

To investigate the non-equilibrium condensation in the supersonic separator, a viscous flow solver with slip model was built and validated by several sets of experiment data. The detailed introduction of the experimental device was discussed.

Then, the flow fluid in the supersonic separator was analyzed. The swirling motion is generated in the vortex generator. The maximum values of tangential velocity and centrifugal acceleration in the separation part are about 65.4 m/s and $7.6\times10^{5}m/s^{2}$, respectively.

Finally, the separation process in supersonic separator was researched. For the gas-droplet two-phase flow formed by non-equilibrium condensation in the supersonic separator, the strong swirls will lead to the liquid droplets separation process. The homogeneous nucleation ratio shows a rapid variation in the downstream position of nozzle throat. Moreover, the droplet behavior of non-equilibrium condensation in the Twister Mark II supersonic separator was discussed in detail.

References

[1] P.B. Machado, J.G. Monteiro, J.L. Medeiros, H.D. Epsom, O.Q. Araujo, Supersonic separation in onshore natural gas dew point plant, J. Nat. Gas Sci. Eng. 6 (2012)43–49.

[2] Y. Yang, C. Wen, S. Wang, Y. Feng, Effect of inlet and outlet flow conditions on natural gas parameters in supersonic separation process, PLoS ONE 9 (2014) e110313.

[3] M. A. Abdi. Computational Fluid Dynamics Study for Flow of Natural Gas through High-pressure Supersonic Nozzles: Part 1. Real Gas Effects and Shockwave[J]. Petroleum Science & Technology, 2008, 26(15):1757-1772.

[4] F. Okimoto, J. M. Brouwer. Supersonic gas conditioning[J]. World Oil, 2002, 223(8):89-91.

[5] B. Prast, B. Lammers, Betting M. CFD for supersonic gas processing [J]. International Journal of Radiation Oncology Biology Physics, 2006, 66(3Suppl):S179-S179.

[6] P. Schinkelshoek, H Epsom. Supersonic Gas Conditioning-Low Pressure Drop TWISTER for NGL Recovery[C]// 2006.

[7] M. Haghighi, K. A. Hawboldt, M. A. Abdi. Supersonic gas separators: Review of latest developments[J]. Journal of Natural Gas Science & Engineering, 2015, 27:109-121.

[8] C. Wen, A. Li, J. H. Walther, et al. Effect of swirling device on flow behavior in a supersonic separator for natural gas dehydration[J]. Separation & Purification Technology, 2016, 168:68-73.

[9] C. Wen, X. Cao, Y. Yang, et al. Numerical simulation of natural gas flows in diffusers for supersonic separators[J]. Energy, 2012, 37(1):195-200.

[10] Y. Yang, C. Wen. CFD modeling of particle behavior in supersonic flows with strong swirls for gas separation[J]. Separation & Purification Technology, 2017, 174:22-28.

[11] Q. Ma. Location Selection of Extra Nuclei Injecting for Inner - Core SGS Device with Droplet Enlargement Measure[J]. Advanced Materials Research, 2012, 516-517:931-934.

[12] A. Karimi, M. A. Abdi. Selective dehydration of high-pressure natural gas using supersonic nozzles[J]. Chemical Engineering & Processing Process Intensification, 2009, 48(1):560-568.

[13] D. Jiang, Q. Eri, C. Wang, et al. Fast and efficient numerical-simulation method for supersonic-gas processing[J]. Journal of Petroleum Technology, 2010, 62(12):71-72.

[14] A. Shahsavand. Optimal Selection of Supersonic Separators Inlet Velocity Components via Maximization of Swirl Strength and Centrifugal Acceleration[J]. Separation Science & Technology, 2015, 50(5):752-759.

[15] V. Alfyorov, L. Bagirov, L. Dmitriev, et al. Supersonic nozzle efficiently separates natural gas components[J]. Oil & Gas Journal, 2005, 103(20):53-58.

[16] C. Wen, Y. Yang, J. H. Walther. Effects of delta wing on the particle flow in a novel gas supersonic separator[J]. Powder Technology, 2016.

[17] M. Haghighi, K. A. Hawboldt, M. A. Abdi. Supersonic gas separators: Review of latest developments[J]. Journal of Natural Gas Science & Engineering, 2015, 27:109-121.

[18] W. Wróblewski, S. Dykas. Two-fluid model with droplet size distribution for condensing steam flows[J]. Energy, 2016, 106:112-120.

[19] H. Ding, C. Wang, C. Chen. Non-equilibrium condensation of water vapor in sonic nozzle[J]. Applied Thermal Engineering, 2014, 71(1):324-334.

[20] H. Ding, C. Wang, G. Wang. Self-excited oscillation of non-equilibrium condensation in critical flow nozzle[J]. Applied Thermal Engineering, 2017, 122.

[21] S. V. Patankar, D. B. Spalding. A calculation procedure for heat, mass and momentum transfer in three-dimensional parabolic flows[J]. International Journal of Heat & Mass Transfer, 1972, 15(10):1787-1806.

[22] K. Elsayed. Design of a novel gas cyclone vortex finder using the adjoint method[J]. Separation & Purification Technology, 2015, 142:274-286.

[23] S. E. Norris, A parallel Navier–Stokes solver for natural convection and free surface flow. doctoral thesis, University of Sydney, 2000.

[24] M. J. Raw, Robustness of coupled algebraic multigrid for the Navier-Stokes equations, AIAA 96-0297, 34th Aerospace and Sciences Meeting & Exhibit, January 15-18 1996, Reno, NV.

[25] C. Wang, H.B. Ding, Q. Liu, H.X. Wang. The Dynamic Compensation of Temperature Sensors in Sonic Nozzle Airflow Standard Facilities Based on Method of Positive Pressur, IEEE International Instrumentation and Measurement Technology Conference, May 2012, pp. 2005-2009.

[26] B. E. Wyslouzil, C. H. Heath, J. L. Cheung. Binary condensation in a supersonic nozzle[J]. Journal of Chemical Physics, 2000, 113(17):7317-7329.